Mendeleev Communications

Mendeleev Commun., 2025, **35**, 699–701

^{119}Sn Mössbauer spectroscopy of nickel zinc orthostannates prepared by self-propagating high-temperature synthesis

Maxim V. Kuznetsov,*[a] Denis A. Pankratov,[b,c] Yurii G. Morozov,[d] Alexey V. Safonov[a] and Olga V. Belousova[d]

[a] *All-Russian Research Institute on Problems of Civil Defence and Emergencies, 121352 Moscow, Russian Federation. E-mail: maxim1968@mail.ru*
[b] *Department of Chemistry, M. V. Lomonosov Moscow State University, 119991 Moscow, Russian Federation. E-mail: pankratov@radio.chem.msu.ru*
[c] *Moscow Institute of Physics and Technology (National Research University), 141700 Dolgoprudny, Moscow Region, Russian Federation*
[d] *A. G. Merzhanov Institute of Structural Macrokinetics and Materials Science, Russian Academy of Sciences, 142432 Chernogolovka, Moscow Region, Russian Federation*

DOI: 10.71267/mencom.7804

Zinc orthostannate (Zn_2SnO_4) and nickel zinc orthostannate ($Zn_{1.2}Ni_{0.8}SnO_4$) were prepared by self-propagating high-temperature synthesis (SHS) and characterized by ^{119}Sn Mössbauer spectroscopy. Both orthostannates are cubic spinels exhibiting defect-induced ferromagnetic behavior due to their microstructures. The Mössbauer spectrum of Zn_2SnO_4 appears as single unresolved doublet [δ = 0.169(3) mm s^{-1}, Δ = 0.45(1) mm s^{-1}], and in the case of $Zn_{1.2}Ni_{0.8}SnO_4$, partial substitution of zinc by nickel is the cause of the appearance of a second doublet of Sn^{4+} [δ = 0.44(9) mm s^{-1}, Δ = 1.62(1) mm s^{-1}] due to an increase in the occupancy of the 5*s* orbital of the corresponding tin atoms and the localization of crystallographic defects near them.

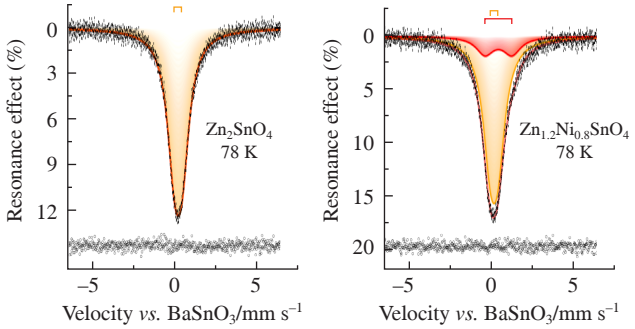

Keywords: self-propagating high-temperature synthesis, SHS, nickel zinc orthostannates, microstructure, X-ray diffraction, Mössbauer spectra, XPS, magnetic measurements.

Previously, as a result of direct self-propagating high-temperature synthesis (SHS), both unsubstituted and nickel-doped cermet materials in the Zn–Sn–O system were obtained and studied by various physicochemical methods.[1,2] Currently, complex stannates attract the attention of researchers due to their unique electrically conductive properties in combination with high mechanical strength, corrosion resistance, magnetic behavior[3] and chemical inertness with respect to various electrolytes.[4–7] In addition, zinc orthostannates have high sensitivity and selectivity towards some potentially hazardous gases, such as ethanol, ammonia, propane, carbon monoxide, *etc.*[8,9]

The combustion process was carried out in air with mechanically ground mixtures of the appropriate metal, metal oxides (used as diluents) and $NaClO_4$.† The precursor materials were combined in stoichiometric quantities according to the following reactions:

$$Zn + ZnO + SnO_2 + 0.25NaClO_4 = Zn_2SnO_4 + 0.25NaCl, \quad (1)$$

$$0.8\,NiO + 1.2Zn + SnO_2 + 0.3NaClO_4 = Zn_{1.2}Ni_{0.8}SnO_4 + 0.3NaCl. \quad (2)$$

The SHS reaction was driven by the exothermic oxidation of Zn metal. Sodium perchlorate was used as the internal oxidizing agent in the reaction. The corresponding metal oxides acted as a heat sink.

Analysis of the obtained materials by powder X-ray diffraction (Figure 1) confirmed that Zn_2SnO_4 and $Zn_{1.2}Ni_{0.8}SnO_4$ have single-phase cubic structures ($m\bar{3}m$) with lattice parameters of 8.657 and 8.608 Å, respectively.

Scanning electron microscope examination‡ of the samples (Figure 2) indicated an open porous morphology with an average particle size of 1 μm for both samples.

The $Zn_{1.2}Ni_{0.8}SnO_4$ and Zn_2SnO_4 samples yielded Raman spectra‡ that were almost identical to those expected. The specific

† All reagents were obtained from Aldrich Chemical Company and were used as supplied. The starting material (~1–2 g) was isostatically pressed under 1 t pressure into pellets of 13 mm in diameter and 2 mm in thickness. A REKROW RK-2060 Micro Torch (UK) was used to ignite the pellets. This promoted the generation of an orange-yellow propagation wave, which travelled at a velocity of 1.0–1.5 mm s^{-1} and reached a maximum temperature of 1350–1500 K. The reaction products were ground and washed with deionized water to remove sodium chloride from the product.

‡ Powder X-ray diffraction measurements were performed on a Bruker Gadds D8 diffractometer using CoKα radiation with a wavelength of 1.79 Å. Scanning electron microscopy of the stannates was carried out on a Phillips XL30 ESEM instrument. Raman spectra were recorded at room temperature using a Renishaw 1000 Raman microscope system equipped with a diode laser operating at 514 nm. The specific surface area of the microstructured powders was studied using four-point measurements of nitrogen physisorption by the BET method on a META Sorbi®-M instrument. Magnetic measurements at 300 K were carried out on an EG&G PARC M4500 vibrating-sample magnetometer.

High-resolution X-ray photoelectron spectroscopy (XPS) was performed on a Thermo monochromated photoelectron spectrometer using monochromatic AlKα radiation. Survey spectra were collected at pass energy of 160 eV, while narrow scans were acquired at pass energy of 40 eV.

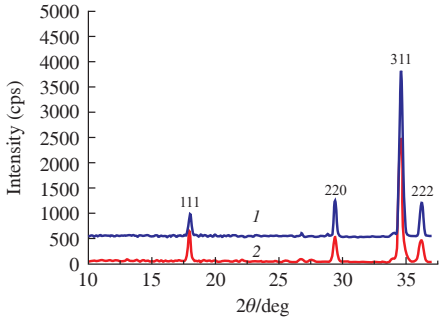

Figure 1 X-ray diffraction patterns of (*1*) $Zn_{1.2}Ni_{0.8}SnO_4$ and (*2*) Zn_2SnO_4 materials.

surface area (*S*) and magnetic characteristics of the produced stannates are presented in Table 1. Structural and magnetic studies‡ have shown that the nature of defects as well as Ni^{2+} ions may be responsible for the magnetic moment of nickel-substituted zinc orthostannate at room temperature.[10] All synthesized materials are ferromagnetics at room temperature with a net saturation magnetization of up to 0.2 emu g^{-1} and a coercivity of 130 Oe. This behavior can be interpreted in terms of the defect structure of the crystal surfaces of the material containing vacancies, interstitials or both of Zn, Sn (Ni) and O, the concentration and degree of mutual interaction of which depends on the synthesis conditions, as it was previously found for the simple binary oxides of Zn and Sn.[4,11] The presence of oxygen vacancies was established using XPS.‡ Their density also increases upon doping with Ni, which is probably accompanied by a d^0 RTFM enhancement. It should be noted that as a result of the experiments with high-temperature treatment (at $T > 1000$ K), a stable high-temperature modification of cubic zinc orthostannate was obtained. To verify the stability of the orthostannate properties over time, their main magnetic characteristics were tested, including after 12 years of storage (see Table 1). It can be concluded that the magnetic characteristics of the samples are stable over time, as are the more magnetically soft characteristics of the undoped sample.

As expected, the XPS spectra of $Zn_{1.2}Ni_{0.8}SnO_4$ powder in the Zn 2*p*, Ni 2*p*, Sn 3*d* and O 1*s* regions indicate the presence of single environments of zinc, tin and nickel in the material. The oxygen scan indicates the presence of two separate environments, consistent with the crystal structure of the material.[1]

The Mössbauer spectra‡ of the studied samples at both temperatures showed very broad resonance lines. The temperature dependences of the shape of these resonance lines and their intensities are very insignificant, so the presence of Sn and SnO in the samples can be excluded. Absorption in these phases occurs in the high-velocity region and is characterized by strong temperature dependences of the *f*-factor (recoil-less fraction).[12]

The Mössbauer spectra of the Zn_2SnO_4 sample at both temperatures [Figure 3(*a*),(*c*)] can be satisfactorily described by unresolved doublets with isomer shifts corresponding to oxygen

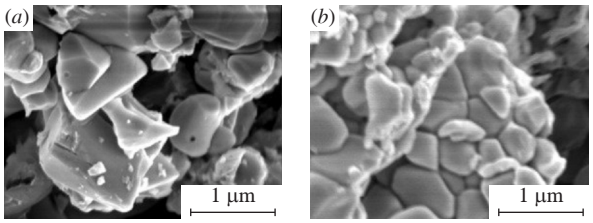

Figure 2 Scanning electron microscopy images of (*a*) Zn_2SnO_4 and (*b*) $Zn_{1.2}Ni_{0.8}SnO_4$ samples.

compounds of Sn^{IV}.[13] The values of the isomer shift and quadrupole splitting calculated from the spectra obtained at room temperature are similar to those for zinc stannate Zn_2SnO_4 with the inverse spinel structure and cannot be attributed to Sn^{IV} oxide.[14,15] This contrasts with the results of a number of other studies, where the Mössbauer spectrum of the corresponding compound was described by two doublets attributed to Sn^{4+} ions in two different octahedral positions.[14,16]

For the samples studied in this work, the model with two doublets turned out to be statistically unacceptable, regardless of the temperature at which the spectrum was recorded. It is also impossible to assume the presence of impurities of another zinc stannate in the sample, for example, metastannate $ZnSnO_3$, since its parameters should obviously be similar to those of isostructural barium and calcium stannates.[17] In addition, $ZnSnO_3$ is a low-temperature modification of zinc stannate, the phase transition of which to the high-temperature modification (Zn_2SnO_4) occurs at temperatures above 770 K. In this case, the formation of a thermodynamically stable high-temperature phase is completed at 1025 K. As mentioned above, the temperatures of combustion processes in the systems under consideration are in the range of 1350–1500 K,† so the formation of a low-temperature modification during their occurrence is impossible. Thus, taking into account the absence of a temperature dependence of quadrupole splitting and an inverse temperature dependence of the line width, we can confidently state that the Mössbauer spectra we obtained relate to Sn^{4+} ions in octahedral positions of a single phase, $Zn[ZnSn]O_4$.

The Mössbauer spectra of $Zn_{1.2}Ni_{0.8}SnO_4$ obtained at two temperatures, despite their similar appearance to the spectra of Zn_2SnO_4, can hardly be satisfactorily described using only one singlet or doublet. When using a model describing the experimental spectrum with a single doublet, systematic deviations from the average value appear in the difference spectrum, which indicates the presence of additional components in the spectrum. Analysis of the probability functions of the isomeric shift distributions for singlets, as well as isomeric shifts and quadrupole offsets for doublets, leads to the same conclusions. In both cases, a bimodal distribution of the hyperfine parameters of the spectra was observed.

Interpretation of Mössbauer spectra of tin is often a difficult and ambiguous task due to the large ratio of the resonance line width to the quadrupole splitting value, which leads to strong cross-correlations of the hyperfine parameters modeling the experimental subspectral data. To describe the spectra of $Zn_{1.2}Ni_{0.8}SnO_4$, we assumed that the main part of the spectrum

Table 1 Characteristics of as-prepared and aged for 12 years Zn–Ni–Sn–O samples with structural defects.

Sample		S/m^2 g^{-1}	σ_s/emu g^{-1}	σ_r/emu g^{-1}	H_c/Oe
Formula	History				
Zn_2SnO_4	As-prepared	1.30	0.198	0.020	130
$Zn_{1.2}Ni_{0.8}SnO_4$	As-prepared	1.60	0.286	0.032	130
Zn_2SnO_4	Aged	1.28	0.165	0.0075	62
$Zn_{1.2}Ni_{0.8}SnO_4$	Aged	1.57	0.277	0.018	75

The data was analyzed using CasaXPSTM software and calibrated against the C 1*s* signal at 284.1 eV attributed to adventitious carbon.

The ^{119}Sn Mössbauer absorption spectra were obtained on an MS-1104Em express Mössbauer spectrometer (ZAO Kordon). The source of γ-radiation was ^{119}Sn in a $CaSnO_3$ matrix with an activity of 1.2 mCi (Ritverc JSC). The spectra were recorded both at room temperature without temperature control and at liquid nitrogen temperature with temperature control. All the spectra were recorded with a noise/signal ratio of 1.3%. Experimental data for high-resolution Mössbauer spectra (1024 points) were processed using the SpectraRelax 2.8 software. The model description of the spectra was carried out by combinations of symmetric doublets with fixed intensity-to-width ratios of resonance lines having a pseudo-Voigt profile. Isomer shifts (δ) are reported relative to $BaSnO_3$.

Table 2 Results of the model description of Mössbauer spectra.[a]

Sample		T = 296(3) K				T = 77.5(5) K			
Formula	Subspectrum	δ/mm s^{-1}	Δ/mm s^{-1}	Γ_{exp}/mm s^{-1}	S# (%)	δ/mm s^{-1}	δ/mm s^{-1}	Γ_{exp}/mm s^{-1}	S# (%)
Zn_2SnO_4	1	0.169(3)	0.45(1)	1.14(1)	100	0.218(2)	0.46(1)	1.10(1)	100
$Zn_{1.2}Ni_{0.8}SnO_4$	1	0.169(f)	0.45(f)	1.13(5)	83(5)	0.218(f)	0.46(f)	1.15(2)	87(2)
	2	0.440(9)	1.62(10)	1.90(1)	17(5)	0.490(9)	1.64(6)	1.19(8)	13(2)

[a] δ is the isomer shift, Δ is the quadrupole splitting, Γ_{exp} is the line width, S# is the relative area of the corresponding subspectrum, and (f) indicates that the value of the parameter is fixed.

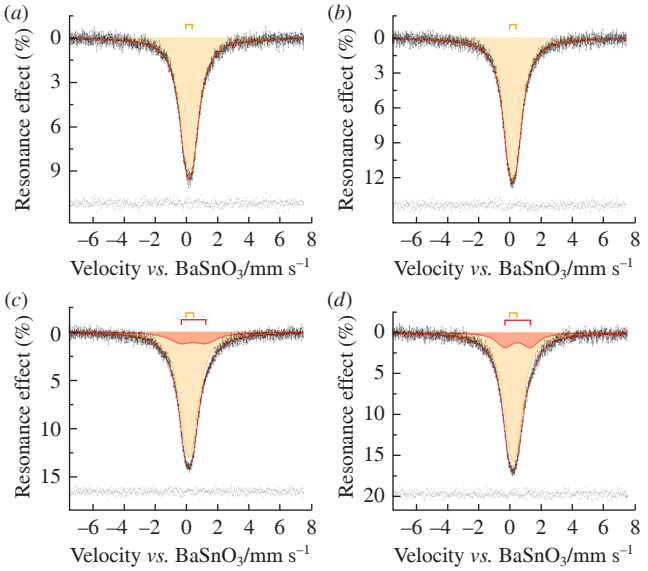

Figure 3 Mössbauer spectra of (*a*),(*c*) Zn_2SnO_4 and (*b*),(*d*) $Zn_{1.2}Ni_{0.8}SnO_4$ at (*a*),(*b*) 296 and (*c*),(*d*) 78 K and the results of their model description. The errors of the experimental points are shown in the figure. The results of subtracting the experimental spectrum from the model spectrum are given at the bottom of all the figures.

should be described by a doublet with parameters similar to those of the doublet describing the spectra of Zn_2SnO_4. In this case, the remaining part of the spectrum can only be described by an additional doublet, also corresponding to Sn^{4+}.[18,19] A significantly increased chemical shift value in this case indicates an increase in the occupancy of the 5*s* orbital of the corresponding tin atoms. A significant value of quadrupole splitting is a sign of a strong distortion of the symmetry of the immediate environment (Table 2). Perhaps, this is due to the localization of crystallographic defects near the tin atoms.

In summary, it was demonstrated that ferromagnetic undoped and nickel-substituted zinc orthostannates prepared by SHS exhibit Mössbauer spectra with one or two doublets corresponding to Sn^{4+}, respectively. The value of the isomer shift and quadrupole splitting of the second doublet can be described taking into account the strong distortion of the symmetry of the local tin environment due to the localization of crystallographic defects. In addition, promising technological approaches have been developed for the synthesis and investigation of the physicochemical characteristics of both undoped and nickel-substituted zinc orthostannates, which are promising from the point of view of their use as a buffer layer in highly efficient solar cells.

The Mössbauer analysis was carried out within the framework of the state assignment of Lomonosov Moscow State University ‘Solution of nuclear energy problems and environmental safety issues, as well as diagnostics of materials using ionizing radiation’ (grant no. 122030200324-1). The authors thank the Development Program of Lomonosov Moscow State University for providing access to the Cryogen-free closed cycle cryostat for Mössbauer spectroscopy CFPR-221-MESS.

References

1 T. Sathitwitayakul, M. V. Kuznetsov, I. P. Parkin and R. Binions, *Sens. Lett.*, 2014, **12**, 1567; https://doi.org/10.1166/sl.2014.3342.
2 T. V. Barinova, I. P. Borovinskaya, V. I. Ratnikov and A. F. Belikova, *Inorg. Mater.*, 2009, **45**, 203; https://doi.org/10.1134/S0020168509020174.
3 A. V. Tyurin, A. V. Khoroshilov, M. A. Ryumin, V. N. Guskov, A. V. Guskov, P. G. Gagarin, G. E. Nikiforova, O. N. Kondrat’eva, K. I. Pechkovskaya, N. N. Efimov, V. M. Gurevich and K. S. Gavrichev, *Russ. J. Inorg. Chem.*, 2020, **65**, 1891; https://doi.org/10.1134/S0036023620120207.
4 Iu. G. Morozov, O. V. Belousova, C. Blanco-Andujar, D. Ortega and M. V. Kuznetsov, *Solid State Sci.*, 2022, **126**, 106854; https://doi.org/10.1016/j.solidstatesciences.2022.106854.
5 M. V. Kuznetsov and A. V. Safonov, *Mater. Chem. Phys.*, 2023, **302**, 127739; https://doi.org/10.1016/j.matchemphys.2023.127739.
6 S. Pavlov and N. Makarov, *MATEC Web Conf.*, 2021, **346**, 02008; https://doi.org/10.1051/matecconf/202134602008.
7 D. A. Antonov, V. V. Anisimov and M. A. Tarasenko, *MATEC Web Conf.*, 2021, **346**, 02012; https://doi.org/10.1051/matecconf/202134602012.
8 T. Sathitwitayakul, M. V. Kuznetsov, I. P. Parkin and R. Binions, *Mater. Lett.*, 2012, **75**, 36; https://doi.org/10.1016/j.matlet.2012.02.003.
9 A. Sivapunniyam, N. Wiromrat, M. T. Z. Myint and J. Dutta, *Sens. Actuators, B*, 2011, **157**, 232; https://doi.org/10.1016/j.snb.2011.03.055.
10 P. R. Chithira and T. J. Teny, *J. Alloys Compd.*, 2018, **766**, 572; https://doi.org/10.1016/j.jallcom.2018.06.336.
11 Iu. G. Morozov, O. V. Belousova, D. Ortega, M.-K. Mafina and M. V. Kuznetcov, *J. Alloys Compd.*, 2015, **633**, 237; https://doi.org/10.1016/j.jallcom.2015.01.285.
12 M. V. Kuznetsov, D. A. Pankratov, I. G. Morozov, I. P. Parkin, A. V. Safonov and O. V. Belousova, *Mendeleev Commun.*, 2021, **31**, 884; https://doi.org/10.1016/j.mencom.2021.11.039.
13 E. G. Ippolitov, T. A. Tripol’skaya, P. V. Prikhodchenko and D. A. Pankratov, *Russ. J. Inorg. Chem.*, 2001, **46**, 851; https://www.researchgate.net/publication/288372831.
14 D. L. Young, D. L. Williamson and T. J. Coutts, *J. Appl. Phys.*, 2002, **91**, 1464; https://doi.org/10.1063/1.1429793.
15 V. Šepelák, S. M. Becker, I. Bergmann, S. Indris, M. Scheuermann, A. Feldhoff, C. Kübel, M. Bruns, N. Stürzl, A. S. Ulrich, M. Ghafari, H. Hahn, C. P. Grey, K. D. Becker and P. Heitjans, *J. Mater. Chem.*, 2012, **22**, 3117; https://doi.org/10.1039/C2JM15427G.
16 D. L. Young, H. Moutinho, Y. Yan and T. J. Coutts, *J. Appl. Phys.*, 2002, **92**, 310; https://doi.org/10.1063/1.1483104.
17 Y. H. Ochoa-Muñoz, J. E. Rodríguez-Páez and R. Mejía de Gutiérrez, *Mater. Chem. Phys.*, 2021, **266**, 124557; https://doi.org/10.1016/j.matchemphys.2021.124557.
18 T. E. Mølholt, H. P. Gunnlaugsson, K. Johnston, R. Mantovan, J. Röder, V. Adoons, A. Mokhles Gerami, H. Masenda, Y. A. Matveyev, M. Ncube, I. Unzueta, K. Bharuth-Ram, H. P. Gislason, P. Krastev, G. Langouche, D. Naidoo, S. Ólafsson, A. Zenkevich and ISOLDE Collaboration, *J. Phys.: Condens. Matter*, 2017, **29**, 155701; https://doi.org/10.1088/1361-648X/aa5e95.
19 G. A. Sundaram, M. Yang, K. Nomura, S. Maniarasu, G. Veerappan, T. Liu and J. Wang, *J. Phys. Chem. C*, 2017, **121**, 6662; https://doi.org/10.1021/acs.jpcc.6b12397.

Received: 18th April 2025; Com. 25/7804